STRUCTURE, DIELECTRIC AND IMPEDANCE PROPERTIES OF BARIUM STRONTIUM SAMARIUM BISMUTH NIOBATE CERAMIC

K. SAMBASIVA RAO, D. MADHAVA PRASAD P. MURALI KRISHNA, T. SWARNA LATHA

Centre for Piezoelectric Transducer Materials, Physics Department, Andhra University,
Visakhapatnam - 530 003, India

E-mail: konapala@sify.com

Frequency and temperature dependence of dielectric permittivity, impedance and electric modulus of Barium Strontium Samarium Bismuth Niobate, $(Ba_{0.1}Sr_{0.81}Sm_{0.06}Bi_2Nb_2O_9$, BSSBN) ceramics have been studied in frequency and temperature range of 45 Hz - 5 MHz and 31-595°C respectively. Simultaneous substitution of Ba and Sm in SBN increases the phase transition temperature of SBN. Cole-Cole plots of impedance in BSSBN ceramic suggest the relaxation to be non Debye type. Variation of grain and grain boundary resistance with temperature reflects the conduction in BSSBN is through grain. Variation of M'' with frequency at different temperatures in the material results that M''_{max} shifts to higher frequency side indicates the presence of temperature relaxation process in the material. The value of stretched exponential parameter, β showed a minimum at T_C and on either side it gives higher values revealing the transverse mode (soft mode) is weakened and restoring force tends to become zero at ferroelectric - paraelectric transition. Near T_C, in ferroelectric region, the activation energies obtained from complex impedance, electric modulus measurements and ac conductivity at 1 KHz are 0.61eV, 0.60eV and 0.63eV respectively. These are typical values for anionic conduction in BSSBN material.

INTRODUCTION

Aurivillius first reported a family of layered bismuth oxides, more than 50 years ago when studying the Bi_2O_3–TiO_2 system [1], now referred to as Aurivillius phase. Shortly afterwards, Smolenski and Subba Rao recognized that many of the Aurivillius phases are ferroelectrics [2,3]. Bismuth layer structured ferroelectrics (BLSF) belong to the Aurivillius family of materials and have the potential for application in sensors, actuators and microelectromechanical (MEM) systems. They are currently being used in FeRAM and DRAM applications [4, 5]. Recently, applications of BLSF such as $SrBi_2Ta_2O_9$ (SBT), $SrBi_2Nb_2O_9$ (SBN) and $SrBi_2(TaNb)_2O_9$ (SBTN) for FeRAM have attracted increase in attention because of their merits of fatigue resistance, lead-free composition and independence of the ferroelectric properties from film thickness [5, 6]. Ferroelectrics have reversible spontaneous polarization making them ideally suited for use in nonvolatile random access memories (NvRAMs). Polarization is due to dipoles that can switch directions spontaneously under the influence of electric field and dipoles are a result of the non-centrosymmetric crystal structure [7, 8]. Previous research has focused on $Pb(Ti, Zr)O_3$ (PZT), but one of the current problem with PZT is the fatigue resistance of the material. PZT thin films tend to degrade most of the initial amount of switching charge ("fatigue") after

10^6-10^8 cycles of full polarization switching [9]. Bismuth layered perovskite materials have high fatigue resistance and are able to withstand 10^{12} erase/rewrite operations [5] and therefore, have attracted an increasing attention for NvRAm applications [4].

The general formula for BLSFs is $Bi_2A_{m-1}B_mO_{m+3}$, where A = Bi, Pb, Na, K, Sr, Ba, rare-earths; B = Ti, Nb, Ta, Fe, Mo, W, Cr and m = 1-6 [10]. This reflects the fact that there exists a good possibility for mutual doping with these various elements or with some other ions to BLSFs. Usually, the doping could be in bismuth oxide layer and/or in perovskite-like units (A or B sites). Efforts have been reported recently to enhance their properties by substitution of the Bi^{3+} by alternative cations. The substitution of cations such as Pb^{2+}, Sb^{2+}, Sn^{2+} or Ti^{4+} [11-13] in $[Bi_2O_2]^{2+}$ layers have been reported by Milan et al. In the perovskite like units, partial substitution of strontium ions by bismuth ions would increase the Curie temperature and improve the dielectric properties in both SBT and SBN [14-16]. Subba Rao reported that the Curie temperature decreases when the size of A site cations in BLSFs increases [17, 18, 3]. Newnham et al. reported that the 10 at% of Sr^{2+} substituted by Ba^{2+} in SBT with lower Curie temperature and reduced distortions in the perovskite units [19]. Properties of barium incorporated SBT thin films were also reported [20, 21]. It was also found that SBN doping with Ca^{2+} resulted in an appreciable increase in the

Curie temperature and a noticeable decrease in the dc conductivity [22]. At B sites, substitution between niobium and tantalum ions was widely studied [23-25]. Takenaka et al. reported the effects of partial substitution of Nb^{5+} for Ti^{4+} as B-site ions on the formation of layer structure for m ≥ 3, compounds and found a BLSFs series for m = 3 [26]. Among BLSFs, SBT and SBN have been the best candidates for nonvolatile memory device because of their fatigue-free properties [5, 27-29].

The above brief review reveals that BLSF materials have potential for device applications. Besides BLSFs, SBN and SBT are also shown to be important materials for device applications. No report on either impedance or modulus spectroscopic work on simultaneous incorporation of Barium and Samarium in SBN is found in the literature.

The objective of the present work is to understand the grain, grain boundary effect on the electrical properties, from impedance, relaxation mechanism from modulus studies, conductivity behavior from both impedance and thermal AC conductivity.

The present article describes the effect of simultaneous incorporation of Ba^{2+} and Sm^{3+} in SBN on structure, dielectric, impedance and modulus, thermal AC conductivity properties.

EXPERIMENTAL

Ceramic sample $Ba_{0.1}Sr_{0.81}Sm_{0.06}Bi_2Nb_2O_9$ (BSSBN) was prepared employing the conventional ceramic sintering technique by using analar grade $BaCO_3$, Sm_2O_3, $SrCO_3$, Bi_2O_3 and Nb_2O_5. The powders were batched in adequate stoichiometric proportions and then ground in an agate mortar for 6-8 hours in methanol based system. The milled powder was calcined at 900°C/2 hours, by placing the mixture in platinum crucible covered with a lid. The rates of heating and cooling of the furnace are 300°C/1 hour. As the reaction is greatly facilitated by heating, cooling and grinding the sample periodically. Hence, the calcinations procedure was repeating thrice causing the reduction of the surface area of the mixture. The effect of grinding is to maintain a high surface area and to bring fresh surface to contact. Therefore, a homogenous solid solution with less particle size may be obtained. The powder obtained after calcinations, ground again and added a binder poly vinyl alcohol (PVA) to bring the particles closer. Then the powder obtained after grinding with PVA has been placed in a pressure molding press that stamps the ceramic powder into discs by applying a pressure of 450 MPa. The pellet was sintered in closed crucible for 1 hour at 1160°C in air. A relative density above 94% was obtained for the sample. The pellet (dia 10mm, thickness 2 mm) was polished, electroded with silver paste and cured at about 600°C for 20 min. Completion of the reaction and formation of the desired compound was checked by X-ray diffraction technique. The XRD spectra were taken on calcined powder of BSSBN at room temperature using CuKα radiation over a wide range of Bragg angles (10° ≤ 2 ≤ 80°). Electrical impedance (Z), phase angle (θ), loss tangent and capacitance (C) were measured as a function of frequency (42 Hz - 5 MHz) and temperature (35-595°C) using a computer controlled LCR Hi-Tester (HIOKI 3532-50), Japan.

RESULTS AND DISCUSSION

XRD

Figure 1 shows the XRD pattern of BSSBN at room temperature. A standard computer program (POWD) has been utilized for the XRD-profile fitting. Good agreement between experimentally observed (d_{obs}) and calculated (d_{cal}) interplanar spacing has been obtained. The patterns indicated that ceramic composition corresponds to a single-phase homogeneous with orthorhombic structure. The lattice parameters are $a = 5.4997$ Å, $b/a = 1.000$ Å and $c = 25.0836$ Å.

Dielectric

The conventional dielectric characterization at 1 KHz showed a permittivity (ε') peak at 505°C, revealing transition temperature (T_C) = 505°C of BSSBN has been shown in Figure 2a. The room temperature permittivity ($ε'_{RT}$) and permittivity at T_C ($ε'_{TC}$) has been found to be 160 and 700 respectively. However, no shift in T_C value has been observed at different frequencies indicating BSSBN belongs to traditional ferroelectrics but not relaxor. The value of T_C in SBN has been reported as 418°C, 420°C and 440°C by different authors [22, 30, 3]. Simultaneous incorporation of 10% Ba^{2+} and 6% La^{3+} also increases the value of T_C, 392°C of SBN to 485°C [31]. Now in the present system, the T_C has been found to be at 505°C. Above Curie point the material follows Curie-Weiss law. The Curie constant has been calculated and found to be 0.79×10^5 °C, which is almost comparable to the reported value [31, 32].

It is obvious from the Figure 2b, tan δ versus temperature, a change in slope has been observed at a particular temperature, 505°C corresponds to the T_C value and is independent of frequency.

Figure 3 shows frequency dependence of the real (ε') and imaginary (ε") parts of dielectric constant at different temperatures. The real part of the dielectric constant, which implies the charge storage, has a strong dispersion in the low frequency region. The imaginary part of the dielectric constant, that is dominated by the conduction of mobile charge, has nearly a single slope.

It can be seen from Figure 3 both the values of ε' and ε" almost start at approximately 300 at 45 Hz and 350°C. As the temperature increases to 500°C, ε' increases to above 1 000, whereas, ε" increases to above 10 000. Also, they intersect at a frequency, 4 KHz. With increase in temperature both ε' and ε" values are increased. Further, increase in temperature results in the shift of the intersection frequency towards higher frequency. This massive rise in ε" indicates that the mechanism of polarization is not the same in the low- and high frequency region. The low frequency dispersion is observed and is understood that the conducting process is due to ion hopping.

Complex impedance spectroscopy

Complex impedance spectroscopy (CIS) is an important tool to investigate the electrical properties of the polycrystalline materials, which have variety of frequency dependent effects associated with heterogeneities. It permits the separation of electric resistivity related to grain, grain boundary and electrode effects on electrical properties [33], and also, allows us to provide the true picture of electrical and dielectric properties. The frequency dependent properties of materials can be described with the help of complex permittivity (ε^*) complex impedance (Z^*), complex admittance (Y^*),
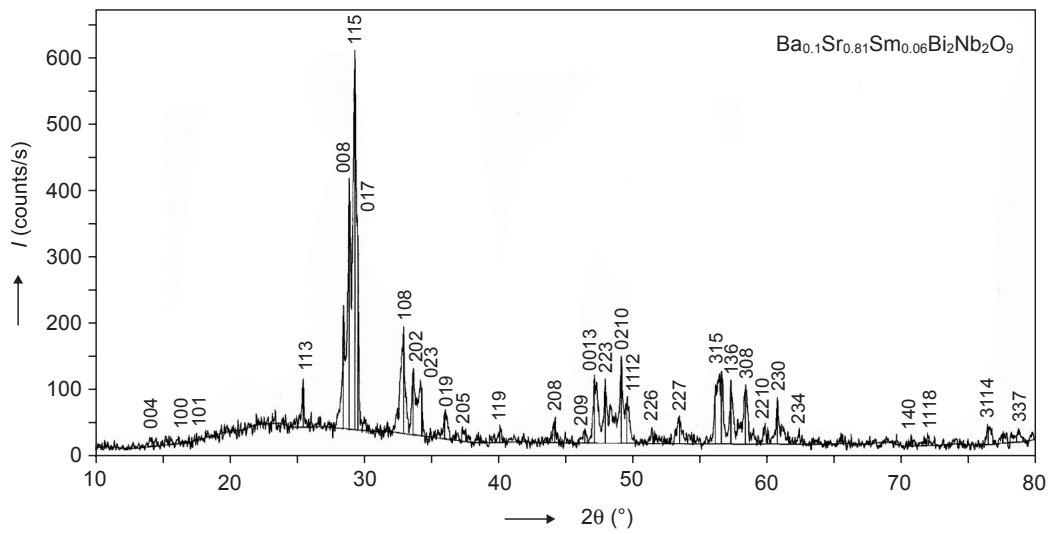

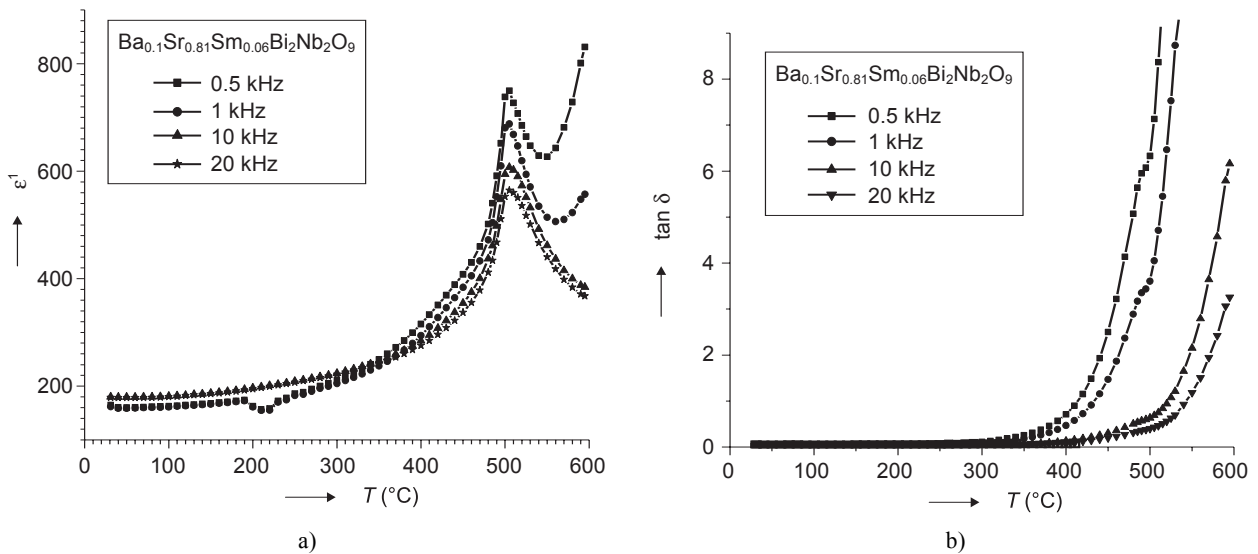Figure 1. X-ray diffraction pattern of BSSBN at room temperature.
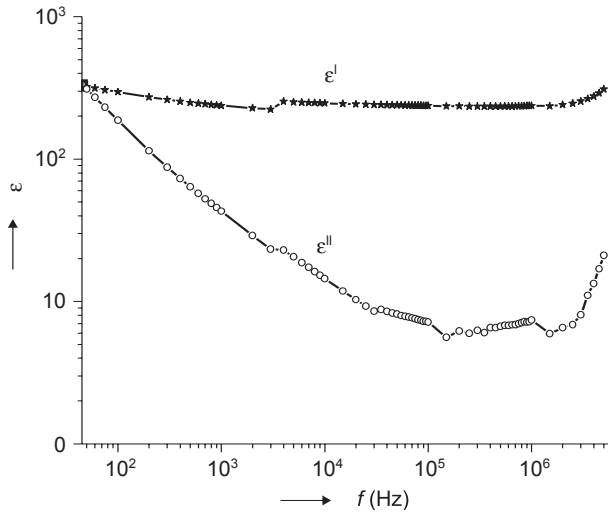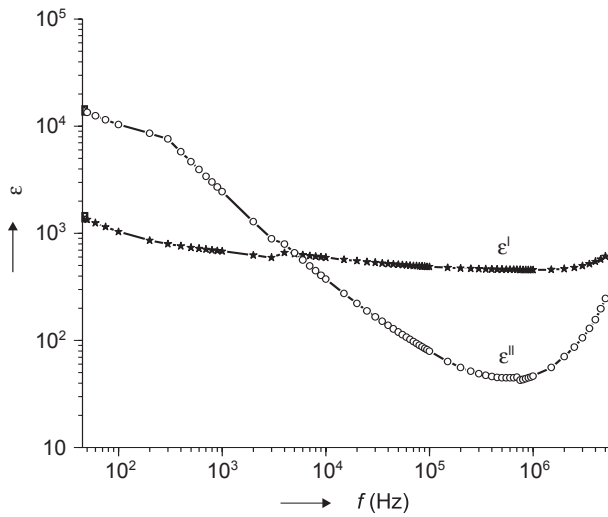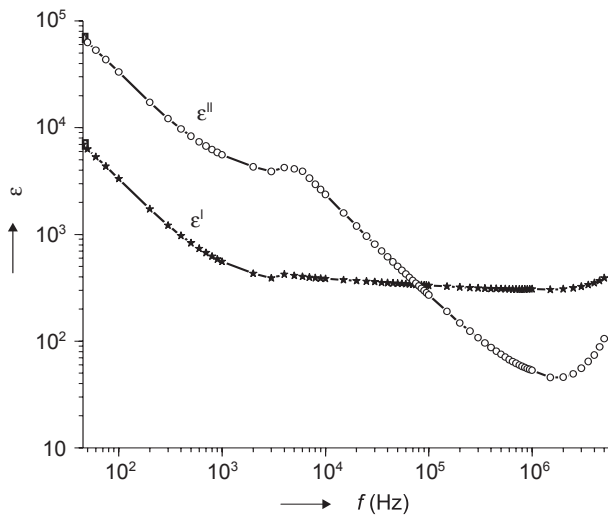

Figure 2. Variation of real dielectric constant (ε') with temperature in BSSBN at various frequencies (a); Variation of tan δ with temperature at different frequencies (b).

a) 350°C

b) 500°C

c) 595°C

Figure 3. The variation of real and imaginary dielectric constant as a function of frequency at different temperatures.

complex electric modulus (M^*) and dielectric loss (tan δ). The following relations relate these parameters to each other

$$\varepsilon^* = \varepsilon' - j\varepsilon'' \tag{1}$$
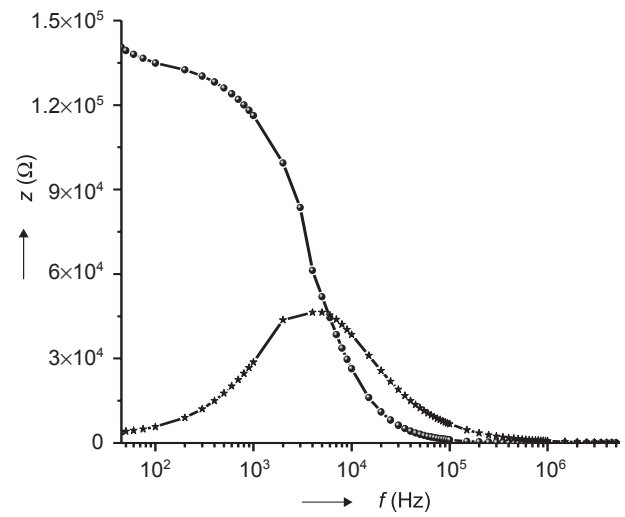$$Z^* = Z' - jZ'' = 1/j\omega C_0\, \varepsilon^* \tag{2}$$
$$M^* = M' - jM'' = 1/\varepsilon^* \tag{3}$$
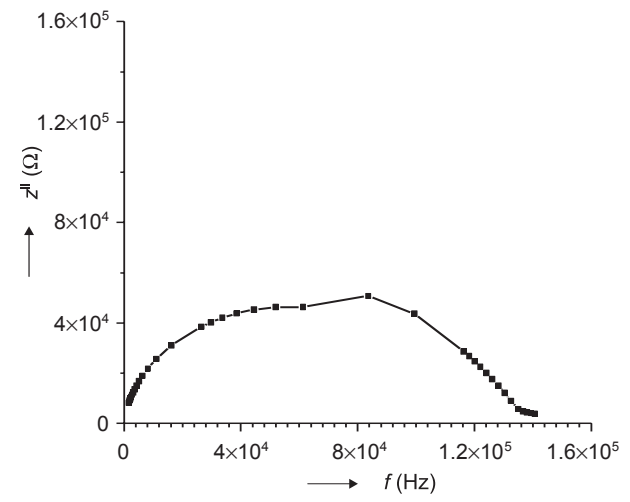$$Y^* = Y' + jY'' = j\omega C_0\, \varepsilon^* \tag{4}$$
$$\tan \delta = \varepsilon''/\varepsilon' = M''/M' = Z'/Z'' = Y'/Y'' \tag{5}$$

where $\omega = 2\pi f$ is the angular frequency; C_0 is the geometrical capacitance, $j = \sqrt{(-1)}$.

Figure 4a shows the frequency dependence of Z' and Z'' at 480°C. As the frequency increases Z'' increases where as Z' decreases. This trend continues upto a particular frequency for which Z'' reaches a maximum

a) 505°C

b) 505°C

Figure 4. Frequency dependence of Z' and Z'' (a), corresponding Argand diagram (b).

value and Z' intersects, for further increase in frequency both Z' and Z'' decrease, and above 10 KHz both values merge with X-axis. This indicates there exists a relaxation phenomenon [34]. Figure 4b shows Argand diagram, (imaginary part of Complex impedance Z^* versus its real part) allows the determination of bulk ohmic resistance as a function of temperature and thus temperature dependence of conductivity [35, 36].

The impedance diagram of the compound is shown in Figure 5 at different temperatures. All the semicircles exhibit some depression degree instead of a semicircle centered on the x-axis. This can be referred to as the Non-Debye type of relaxation in which there is a distribution of relaxation times. This non-ideal behavior can be correlated to several factors, such as grain orientation, grain boundary, stress- strain phenomena and atomic defect distribution. The presence of two semicircles at higher temperature exhibits the presence of both grain interior (bulk property) and grain boundary effect. The contribution positioned at low frequency corresponds to the grain boundary response and in the high frequency, it corresponds to bulk property of the material. The depression of the semicircle is considered as further evidence of polarization phenomena with a distribution of relaxation times. The assignment of the two semicircular arcs to the electrical response, is due to the grain interior and grain boundary, and can be considered to be consistent with the "brick-layer model" for polycrystalline samples [33]. Each semicircle can be represented by a parallel RC circuit that corresponds to the individual component of the material. The intercept of the semicircle on the real axis gives the resistance of the corresponding component contributing towards the impedance of the sample.
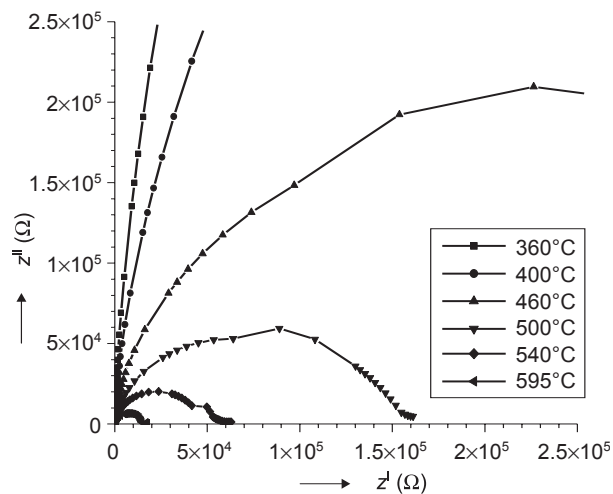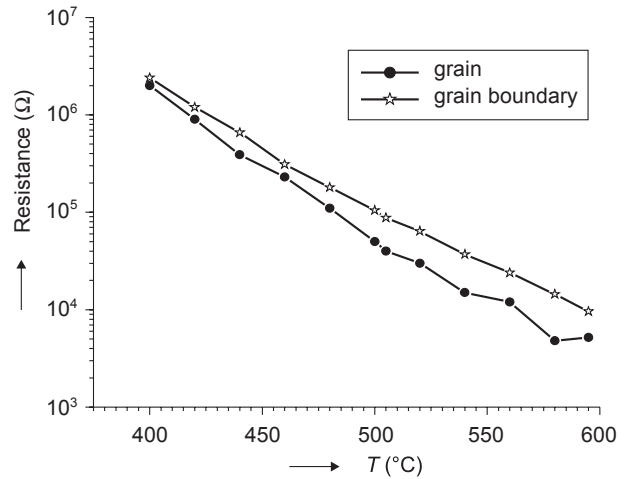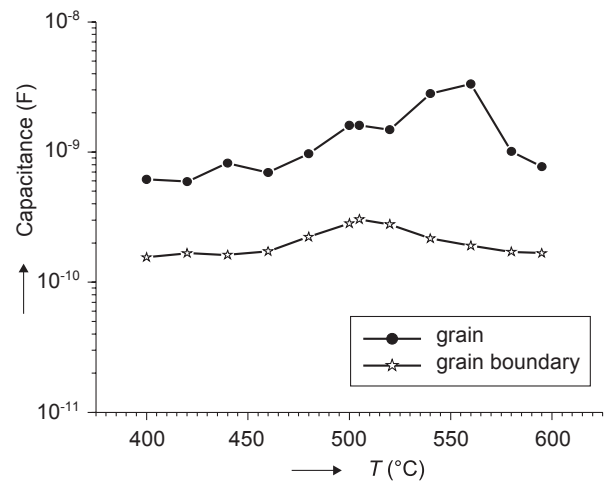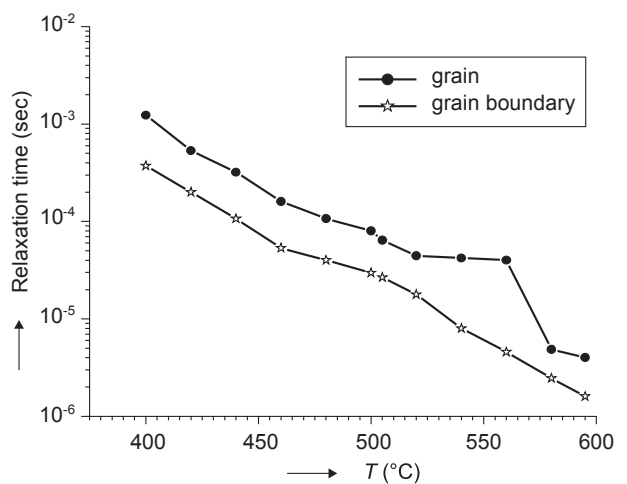

a)

b)

Figure 5. Cole-Cole plots for BSSBN at different temperatures.

c)

Figure 6. Dependance of resistance, capacitance and relaxation time of grain and grain boundary with temperature BSSBN.

The intercepts of the two semicircles are used to calculate the bulk resistance (R_b) and grain boundary resistance (R_{gb}) while the corresponding frequency value evaluated from the apex of the semicircles have been used to calculate the bulk (C_b) and grain boundary capacitance (C_{gb}) using the relation, $\omega_{max}C_bR_b = 1$ or $\omega_{max}C_{gb}R_{gb} = 1$ for a parallel combination of R and C. As temperature increases, both the grain resistance (R_b) and grain boundary resistance (R_{gb}) is found to decrease, indicated by a shift in the radius of the semicircular arcs towards left side on the real (Z') axis.

Figure 6 shows variation of R_b, R_{gb}, C_b and C_{gb}, grain relaxation time, τ_b, and grain boundary relaxation time, τ_{gb} with temperature. It is evident from the Figure 6a that at lower temperature (at 400°C) R_b and R_{gb} having almost the same value. As the temperature increases the R_{gb} is found higher than R_b. From Figure 6b C_b is found to less than C_{gb}. From Figure 6c it is observed that τ_b and τ_{gb} with temperature shows a decrease of relaxation time with increase in temperature. The values of R_b, R_{gb}, ε_b, ε_{gb} are plotted against inverse of temperature yield Arrhenius plots. Slopes of these plots give grain and grain boundary conduction and relaxation activation energies respectively. These values are given in Table 1. From the Table 1, it is observed that $E_{gb} > E_b$ in the temperature range 400-595°C. From the Figure 6a, it is seen that the grain boundary resist-

ance is higher than grain resistance. From Figure 6c, the grain boundary relaxation time appears to be larger than grain. In view of these facts in the present sample, it appears that the conduction is mainly through grain rather than grain boundary.

The loss spectrum (i.e., Z'' versus frequency) of the compound at a different temperature is given in Figure 7a. The asymmetric broadening of the peaks suggests the presence of electrical process in the material with spread of relaxation time (indicated by peak width). The relaxation species may possibly be due to presence of electron at low temperature and defects/vacancies at higher temperature. The magnitude of existing peaks (Z'') decreases gradually with increase in frequency and temperature and finally merges in high frequency domain, which indicates the presence of space charge polarization effects at lower frequency and at higher temperature.

Figure 7b shows the variation of real part of impedance (i.e., Z') as a function of frequency at different temperature. It was found from Figure 7b that Z' values decreases with increase of temperature indicating reduction of grains, grains boundaries and electrode interface resistance. It is also observed that the value of Z' decreases till a certain fixed frequency up to 10 kHz and attain a constant value.

Table 1. Activation energy values (eV) for conduction (E) and relaxation (ε) for grain (b) and grain boundary (gb).

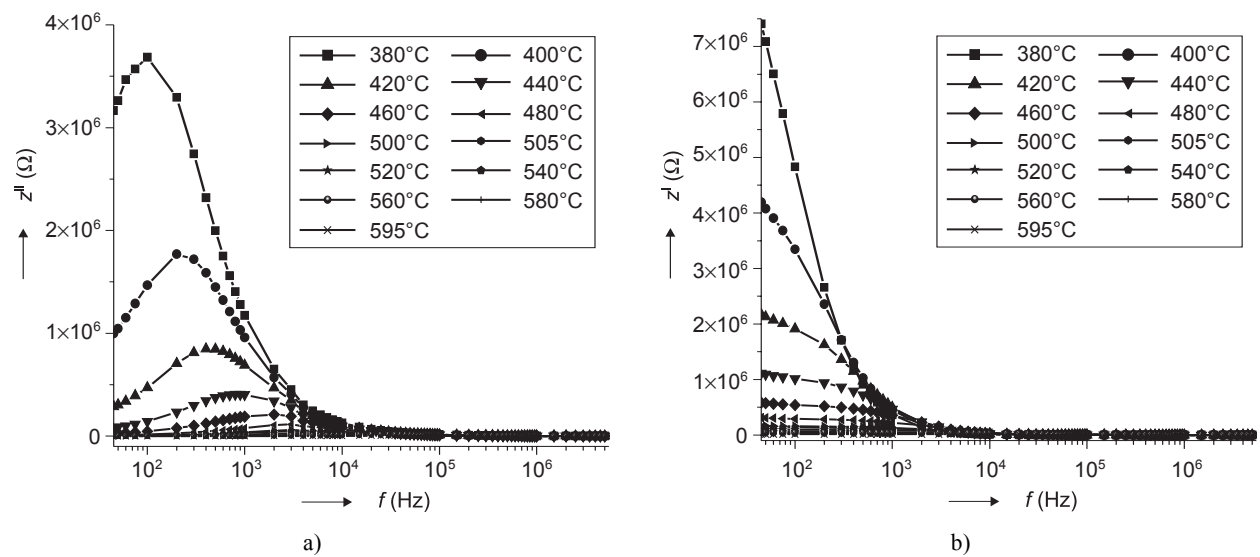| Composition	Grain conduction activation energy, E_b (eV)		Grain boundary conduction activation energy, E_{gb} (eV)		Grain relaxation activation energy, ε_b (eV)		Grain boundary relaxation activation energy, ε_{gb} (eV)	
	400-4800C	520-5950C	400-4800C	520-5950C	400-4800C	520-5950C	400-4800C	520-5950C
BSSBN	0.80	0.61	0.90	0.63	0.52	0.70	0.59	0.86

Figure 7. Variation of Imaginary Z'' (a) and real Z' (b) part of impedance of BSSBN with frequency at different temperatures.

Figure 8a shows the normalized imaginary parts Z''/Z''_{max} of impedance as a function of frequency in BSSBN at several temperatures. It is evident from the Figure 8a that as the temperature increases the peak frequency of Z''/Z''_{max} shifts towards higher frequency side revealing that at high temperatures triggers another relaxation process. The Z''/Z''_{max} parameter exhibits a peak with a slightly asymmetric degree at each temperature especially at higher temperatures. At the peak the relaxation is defined by the condition

$$\omega_m\tau_m = 1 \qquad (6)$$

where τ_m is relaxation time at the peak.

Figure 8b shows the variation of relaxation time (log τ) with inverse of temperature ($10^3/T$). In a relaxation system, the relaxation time (τ) can be calculated from Z'' versus log f plots using the relation:

$$\tau = 1/\omega = 1/2 \ \pi f_{max} \qquad (7)$$

where f_{max} is the relaxation frequency. It is observed that the value of τ found to be decreasing with increasing temperature. The activation energy (E_a) of this compound has been calculated from the Arrhenius relation:

$$\tau = \tau_0 \exp(-E_a/kT) \qquad (8)$$

where τ_0 is the pre-exponential factor, k the Boltzamann constant and T is the absolute temperature. The value of activation energy found to be in ferro and para regions 0.65 and 0.74 eV respectively. An anomaly has bee observed at particular temperature, 505°C which is coincides with the T_C of the material.

Complex Electric Modulus Spectroscopy

The modulus formalism can be used to study the relaxation mechanism in the material. In the modulus formalism, an electric modulus $M*$ is defined in terms of reciprocal of the complex permittivity $\varepsilon*$ in accordance with the Equation (3). The frequency dependence of M' and M'' for the sample at different temperatures is shown in Figure 9. M' shows a dispersion tending to a constant value at higher frequencies, where as M'' exhibits a peak (M''_{max}) centered at the dispersion of M'. Also, it is seen from the Figure 9b that the value of M''_{max} decreases and shifts towards higher frequency side as temperature increases. Further, increase in temperature, M''_{max} begins to increase. It reveals that at T_C, M''_{max} be a minimum value. The shift in M''max indicates the presence of temperature relaxation process in the material.

Figure 10 shows the Arrhenius plot of relaxational angular frequency, $\omega_p = \omega_0 \exp(-E/KT)$ as a function of reciprocal of temperature, where ω_0 and T are the pre-exponential factor of relaxational angular frequency and the absolute temperature. Above and below the phase transition temperature, the two distinct slopes of activation energy obtained from Arrhenius plot were found. The activation energies of above (520-595°C) and below (400-480°C) the phase transition temperature are 0.77eV and 0.60 eV respectively.
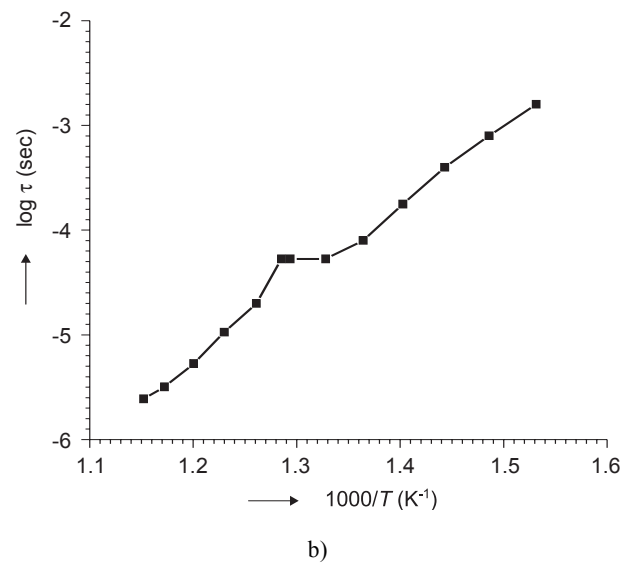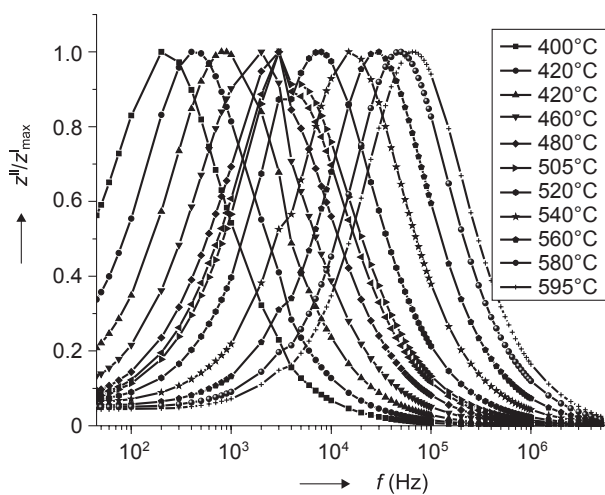

Figure 8. Normalized imaginary parts, Z''/Z''_{max} (a) of impedance as a function of frequency and Variation of relaxation time (log τ) with inverse of temperature $10^3/T$ (b).

DC Conductivity

Electrical conduction (σ_{dc}) is a thermally activated process and follows the Arrhenius law. Figure 11 shows the Arrhenius plot of the dc conductivity evaluated from the impedance plots of BSSBN sample as a function of temperature and the corresponding activation energy values are found to be in ferro and para regions 0.61 eV and 0.80 eV respectively, it may be interpreted as the motion of oxygen vacancies and are consistent with those obtained by the present impedance studies and

also with earlier reports [37]. Oxygen vacancies are considered to be the most mobile charge carriers in layered pervoskite ferroelectrics like SBN and SBT. The evaporation of bismuth oxide in layered pervoskite would lead to oxygen vacancies.

β - Parameter

The electric field relaxation due to ion motion is generally described by the Kohlrausch function $\phi(t) = \exp [-(t/\tau_\sigma)^\beta]$ ($0 \leq \beta \leq 1$) [38-41], where τ_σ and β are the stretched exponential functions, the conductivity
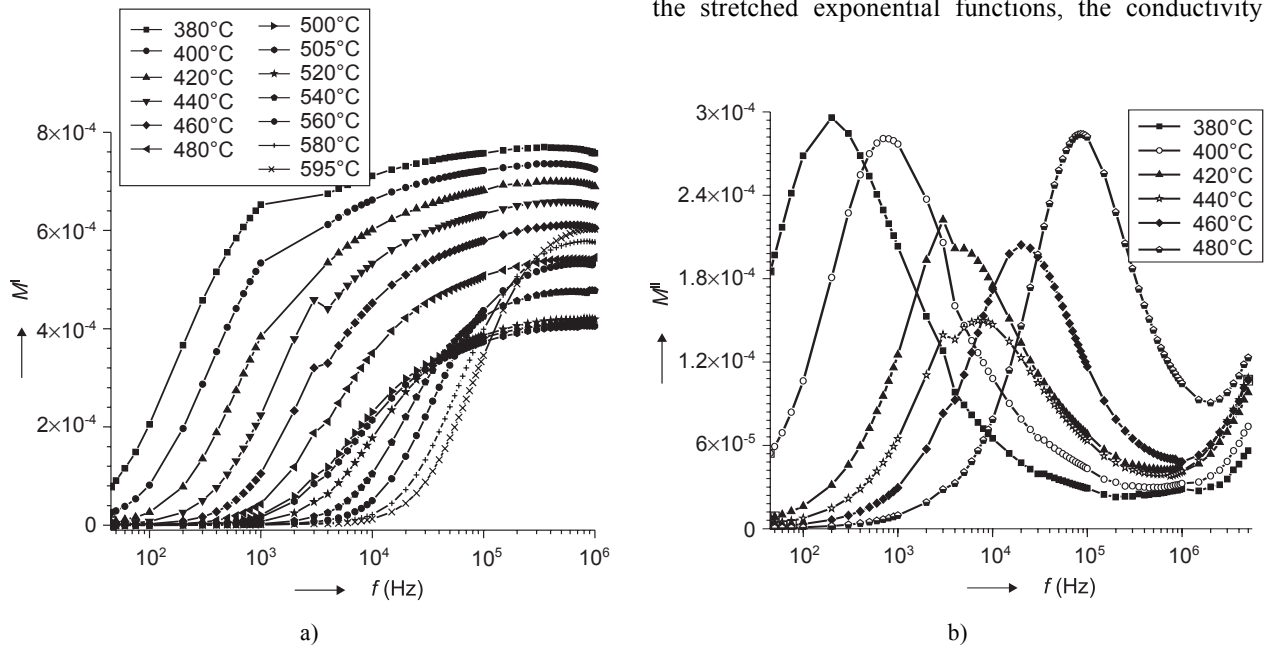
Figure 9. Variation of real part of electrical modulus (M') with frequency (a) and variation of imaginary part of electrical modulus (M") with frequency in BSSBN (b).
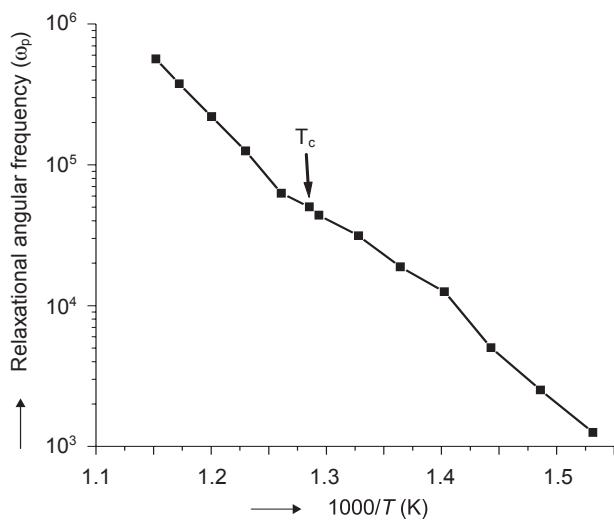
Figure 10. The Arrhenius plot of relaxational angular frequency ω_p as function of inverse temperature.
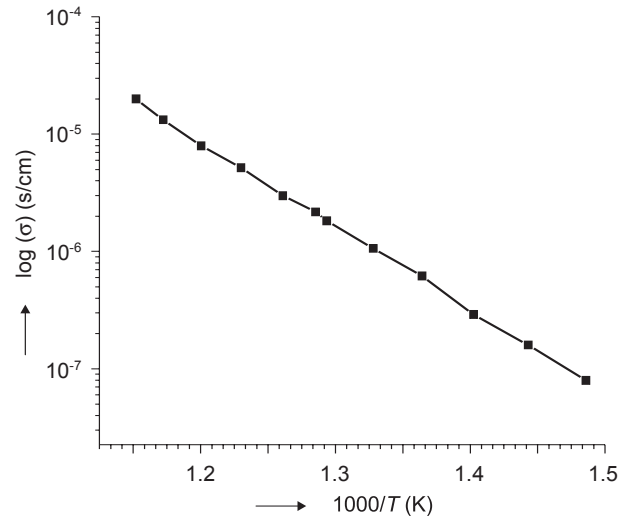
Figure 11. Arrhenius plot for dc conductivity (σ) of BSSBN ceramic.

relaxation time and Kohlrausch exponent respectively. Smaller the value of β the greater the deviation with respect to Debye-type relaxation. The β parameter is most often interpreted as a result of correlated motions between ions. This is the jump of the mobile ion in a material cannot be treated as an isolated event. It results in a time - dependent motion of other charge carriers in the surroundings. The value of β parameter becomes smaller as the cooperation between charge carriers is more extended. For very small charge carriers concentrations, the conductivity is essentially characterize by independent jumps, where as when the mobile ion concentration increases, the coupling between charge carriers is more extended. In both glasses and crystalline ionic conductors, the coupling of charge carriers is reflected by a value of β close to 0.5 [41, 42].
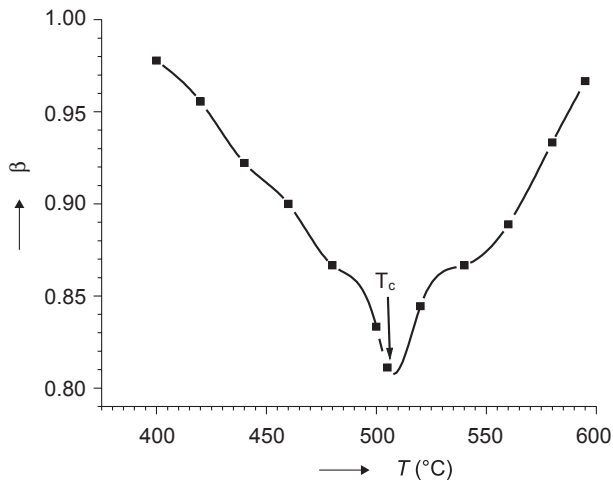
The β parameter in the BSSBN was established as a function of temperature (400-595°C) using impedance formalism. The value of β was determined by fitting the circular arc $Z'' = f(Z')$, the center of semi circle displaced below the x-axis. The above fit allows us to determine the value of depression angle, ϕ and thus β as $\phi = (1 - \beta)\pi/2$. Variation of stretched parameter β with temperature in BSSBN which covers transition temperature of material is shown in Figure 12. It is evident from the figure that β takes a minimum value of 0.81 at 505°C which corresponds to T_C. Then β increases with temperature and takes a maximum value of 0.966 at 595°C. It is obvious from the variation of activation energies obtained from impedance plots and parameter β near T_C, the dynamic process is different from that of apart from phase transition temperature. According to lattice dynamics theory one of the transverse mode (soft mode) is weakend and the restoring force tends to become zero at ferroelectric- paraelectric transition [43]. Therefore, if one assumes that the charge carriers couples with soft mode, one may expect that the charge carriers become mobile at the phase transition temperature.

Figure 12. Stretched exponential parameter β as a function of temperature.

AC Conductivity

Figure 13 shows frequency dependence of ac conductivity (σ^l) at various temperatures. It can be seen that in low frequencies and high temperatures we observe plateaus of σ^l, i.e. frequency independent values of conductivity, which corresponds to the dc conductivity, σ_{dc}. The observed frequency dependent conductivity can be described with the equation [44]:

$$\sigma(\omega) = \sigma_0 + A\omega^s \qquad (9)$$
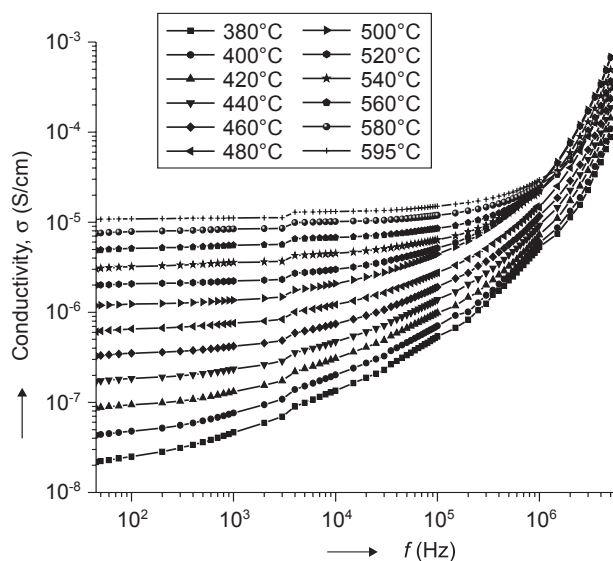
Figure 13. Frequency dependence of real part of AC conductivity σ' at various temperatures.
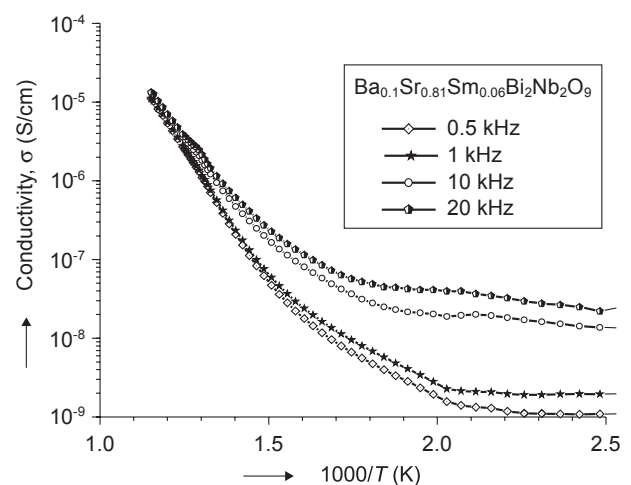

Figure 14. Variation of AC conductivity as function of inverse of temperature.

Thermal behavior of AC conductivity of BSSBN is shown in Figure 14. It is seen from the figure that an anomaly has been observed at a particular temperature, which corresponds to the TC in the sample. Further, the conductivity values at room temperature are found to be order of 10^{-9}. Also, it is observed that the conductivity is found to increase with increase in temperature. The change in slope of curve will reflect a change in the conductivity phenomenon in para and Ferro regions. The change in slope observed in conductivity plots suggests that it can be broadly divided into three regions, which are 320-400°C, 430-490°C and 510-580°C. It is noted that the conductivity curves at different frequencies found to merge at higher temperatures, at these temperature regions the onset of intrinsic conductivity takes place in the material.

The activation energy values in three temperature regions have been given in the Table 2. It is evident from the table that in the ferroelectric region (430-490°C) the value of the activation energy 0.63 eV coincides with the value, 0.61 eV obtained from Dc conductivity. The activation energies obtained from the experiment are typical values for ionic conductivity.

Table 2. AC conductivity activation energy values in BSSBN.

Composition	BSSBN			
Temperature range (°C)	20KHz	10KHz	1KHz	500Hz
320-400	0.29eV	0.22eV	0.28eV	0.25eV
430-490	0.33eV	0.43eV	0.63eV	0.56eV
510-580	0.43eV	0.47eV	0.73eV	0.67eV

CONCLUSION

The temperature and frequency dependence of the dielectric permitivity, impedance and electric modulus in BSSBN have been studied. XRD analysis in BSSBN showed the Orthorhombic crystal structure of SBN is preserved but with slight changes to the lattice parameters. Simultaneous incorporation of Ba and Sm in SBN increases the phase transition temperature of BSSBN. Cole-Cole plots of impedance in BSSBN ceramic suggest the relaxation to be non of Debye type. It follows from the variation of grain and grain boundary resistance with temperature that the electrical conductance is through the grain. Variation of M'' with frequency at different temperatures in BSSBN results that M''_{max} shifts to higher frequency side and M''_{max} decreased with increase in temperature. At T_C M''_{max} is minimum, further increase in temperature M''_{max} increases. The shift in M''_{max} indicates the presence of temperature relaxation process in the material. The value of stretched exponential parameter, β showed a

minimum at T_C and on either side it gives higher values revealing the transverse mode (soft mode) is weakened and restoring force tends to become zero at ferroelectric - paraelectric transition. Near T_C, in ferroelectric regoin the activation energies obtained from complex impedance, electric modulus studies and ac conductivity activation energy at 1 KHz are 0.61 eV, 0.60 eV and 0.63 eV respectively are typical values for an ionic conduction in BSSBN.

References

1. Aurivillius B.: Ark. Kemi *1*, 499 (1949).
2. Smolenski G. A., Isupov V. A., Agranaskaya A. I.: Sov. Phys.Solid State *3*, 561 (1959). (Engl. Transl.)
3. Subba Rao E. C.: J.Phys.Chem.Solids *23*, 665 (1962).
4. Scott J. F., De Araujo C. A. P.: Science *24*, 6 (1989).
5. de Araujo C. A. P., Cuchiaro J. D., Mc Millan L. D., Scott M. C., Scott J. F.: Nature *374*, 627 (1995).
6. Cao G. Z. in: *Advances in Materials Science and applications*, p.86, Ed.: Shi D. L., Tsinghua University Press and Springer - Verlag, Beejing 2001.
7. Jona F., Shirane G.: *Ferroelectric crystals*, Pergamon, New York 1962.
8. Jaffe B., Cook W. R., Jaffe H.: *Piezoelectric ceramics*, Academic Press, New York 1971.
9. Watanabe H., Mihira T.: Jpn.J.Appl.Phys. *34*, 5420 (1995).
10. Robertson J., Chen C. W., Warren W. L., Gutleben C. C.: Appl.Phys.Lett. *69*, 1704 (1996).
11. Milan P., Reminez A., Castro A.: J.Mater.Sci.Lett. *14*, 1657 (1995).
12. Duran -Martin P., Castro A., Milan P., Jimenez B.: J.Mater. Res. *13*, 2565 (1998).
13. Milan P., Castro A., Torrance J. B.: Mater.Res.Bull. *28*, 117 (1993).
14. Atsuki T., Soyama N., Yonezawa T., Ogi K.: Jpn.J.Appl. Phys. *34*, 5096 (1995).
15. Noguchi T., Hase T., Miyasaka Y.: Jpn.J.Appl.Phys. *35*, 4900 (1996).
16. Tsai H., Lin P., Tseng T.: Appl.Phys.Lett. *72*, 1787 (1998).
17. Subba Rao E. C.: J.Chem.Phys. *34*, 695 (1961).
18. Subba Rao E. C.: Phys.Rev. *122*, 804 (1961).
19. Newnham R. E., Wolf R. W., Horsey R. S., Diaz - Colon F. A., Kay M. I.: Mater.Res.Bull. *8*, 1183 (1973).
20. Liu C. H., Wen C. Y.: Mater.Res.Soc.Symp.Proc. *541*, 229 (1999).
21. Liu C. H., Wen C. Y.: J.Eur.Ceram.Soc. *20*, 739 (2000).
22. Forbess M. J., Seraji S., Wu Y., Nguyen C. P., Cao G. Z.: Appl.Phys.Lett. *76*, 2934 (2000).
23. Watanabe H., Mihira T., Yoshimori H., de Araujo C. A. P.: Jpn.J.Appl.Phys. *34*, 5240 (1995).
24. Desu S.B., Vijay D.P.: Mater.Sci.Eng. B *32*, 83 (1995).
25. Desu S. B., Li T.: Mater.Sci.Eng. B *34*, L4 (1995).
26. Takenaka T., Gotoh T., Mutoh S., Sasaki T.: Jpn.J.Appl. Phys. *34*, 5384 (1995).
27. Mihira T., Yoshimori Y., Watanabe H., de Araujo C. A. P.: Jpn.J.Appl.Phys. *34*, 5233 (1995).
28. Scott J. F. in: *Thin film ferroelectric materials and devices*, Ed.: Ramesh R., p.115, Kluwer, Norwell 1997.
29. Suzuki M.: J.Ceram.Soc.Jpn. *103*, 1088 (1995).

30. Smolenski G. A., Isupov V. A., Agranovskaya A. I.: Fiz. Tverdogo Tela *3*, 895 (1961).

31. Sambasiva Rao K., Madhava Prasad D., Murali Krishna P., Tilak B., Varadarajulu K. Ch.: Mat.Sci.Eng. *B 133*, 141 (2006).

32. Liu J., Zou G., Yang H., Cui Q.: Solid State Comm. *90*, 365 (1994).

33. MacDonald J. R.: *Impedance Spectroscopy*, Wiley, New York 1987.

34. Hornebecq V., Reau J. M., Ravez J.: Solid State Ionics *127*, 231 (2000).

35. Cole K. S., Cole R. H.: J.Chem.Phys. *9*, 341 (1941).

36. Bauerle J. E.: J.Phys.Chem.Solids *30*, 2657 (1969).

37. Chen T. C., Thio C., Desu S. B.: J.Mater.Res. *12*, 2628 (1997).

38. Williams G., Watts D. C.: Trans. Fraday Soc. *23*, 625 (1970).

39. Nagai K. L., Martin S. W.: Phys.Rev. *B 40*, 10050 (1989).

40. Howell F. S., Bose R. A., Macedo P. B., Moynihan C. T.: J.Phys.Chem. *78*, 639 (1974).

41. Reqa J. M., Rossignol S., Tanguy B., Paris M. A., Rojo J. M.: J.Solid State Ionics *80*, 283 (1995).

42. Zouari N., Mnif M., Khemakhem H., Mhiri T., Daoud A.: Solid State Ionics *110*, 269 (1998).

43. Zhigao L., Bonnet J. P., Ravez J., Reau J. M., Hagenmuller R.: Phys.Chem.Solids *53*, 1 (1992).

44. Jonseher A. K.: *Dielectric Relaxation in Solids*, Chelsea Dielectric Press, London 1983.

STRUKTURA, DIELEKTRICKÉ VLASTNOSTI
A IMPEDANCE KERAMICKÉHO MATERIÁLU
NA BÁZI NIOBÁTU BARYA, STRONCIA, SAMARIA
A BIZMUTU

K. SAMBASIVA RAO, D. MADHAVA PRASAD,
P. MURALI KRISHNA, T. SWARNA LATHA

Centre for Piezoelectric Transducer Materials,
Physics Department, Andhra University,
Visakhapatnam - 530 003, India

Frekvenční a teplotní závislost dielektrické permitivity, impedance a elektrického modulu keramického materiálu na bázi niobátu barya, stroncia, samaria a bizmutu ($Ba_{0.1}Sr_{0.81}Sm_{0.06}Bi_2Nb_2O_9$, BSSBN) byly studovány v rozsahu frekvence 45 Hz - 5 MHz a teploty 31-595°C. Současné nahrazení Ba a Sm v SBN zvyšuje teplotu fázového přechodu SBN. Vykreslení impedance Cole-Cole v keramice BSSBN ukazuje na uvolnění jiného typu než Debye. Změna zrna a odolnosti hranic zrna vzhledem k teplotě odráží vodivost v BSSBN v zrnech. Změna M'' s frekvencí při různých teplotách v materiálu vede k tomu, že M''_{max} se posouvá na vyšší frekvenci, což naznačuje přítomnost procesu teplotního uvolnění v materiálu. Hodnota prodlouženého exponenciálního parametru β ukazuje minimální hodnotu při T_C a na obou stranách poskytuje vyšší hodnoty, které prokazují, že příčný režim (měkký režim) je oslaben a obnovující síla má tendenci klesat k nule na feroelektrickém-paraelektrickém přechodu. V blízkosti T_C, ve feroelektrické oblasti, dosahují aktivační energie získané na základě komplexních měření impedance a elektrického modulu a vodivosti střídavého proudu při frekvenci 1 kHz hodnot 0,61 eV, 0,60 eV a 0,63 eV. To jsou typické hodnoty pro aniontovou vodivost v materiálu BSSBN.